Supporting information

Highly selective aromatization of octane over Pt-Zn/UZSM-5: The effect of Pt-Zn interaction and Pt position

Peng He[a], Yunlei Chen[c,d], Jack Jarvis[a], Shijun Meng[a], Lijia Liu*[b], Xiaodong Wen[c,d], Hua Song*[a]

[a] Department of Chemical and Petroleum Engineering, University of Calgary, 2500 University Dr NW, Calgary, Alberta T2N 1N4, Canada

[b] Jiangsu Key Laboratory for Carbon-Based Functional Materials & Devices, Institute of Functional Nano and Soft Materials (FUNSOM), Soochow University, Suzhou, Jiangsu, 215123, China

[c] State Key Laboratory of Coal Conversion, Institute of Coal Chemistry, Chinese Academy of Sciences, Taiyuan, Shanxi 030001, China

[d] National Energy Center for Coal to Clean Fuel, Synfuels China Co., Ltd, Huairou District, Beijing 101400, China

*Corresponding author

Fax: +1 (403) 284-4852; Tel: +1 (403) 220-3792;

E-mail: sonh@ucalgary.ca

Table of Contents

1. Experimental

1.1 Theoretical calculation

The DFT calculations of the reaction intermediates were based on the zeolite MFI (ZSM-5) structure with an orthorhombic crystal structure with space group *Pnma* (a = 20.09 Å, b= 19.74 Å and c = 13.14 Å). The general formula of zeolite MFI with pure silicon component is $Si_{96}O_{192}$. The MFI zeolite framework contains twelve crystallographically distinct tetrahedral T sites. The topology is a three-dimensional framework consisting of two 10-ring channels, where the straight channels (5.1–5.5 Å) are cross-connected with the zigzag channels (5.3–5.6 Å). The maximum diameter of sphere that can be included in the channel intersections is 6.36 Å[1]. Previous reports have demonstrated that aluminum was preferential to locate at channel intersection using synthetic methods of zeolite MFI reported in this work[2] and Pt metal tended to aggregate near Al atoms in the inner pore of zeolites. Considering the size of channel intersection, Pt_8 cluster (~5.0 Å) was adopted to interact with Al at T5 site of channel intersection. To investigate the effect of Pt distribution on catalytic performance of Pt/ZSM5, Pt(111) surface was adopted to represent Pt particles on the outer surface of zeolite.

The DFT calculation of the Zn and Pt atoms at different positions was conducted by using DMol3 module in Materials Studio. B3LYP was selected as the exchange-correlation functional. The basis set DNP was used in the calculation. The calculations are carried out without temperature correction, i.e., at T = 0 K. By using this basis set, the effect of occupied atomic orbital and valence atomic orbital have been considered. A polarization p-function on all hydrogen atoms was applied. Therefore, this basis set could provide reasonable accuracy with acceptable computational cost, which was commonly used in DFT calculation for ZSM-5 [3]. During geometry optimization, the tolerances of energy, gradient and displacement convergence were 2×10^{-5} Ha, 4×10^{-3} Ha/Å and

5 × 10^{-3} Å, respectively. The initial ZSM-5 structure was obtained from the database of International Zeolite Association (IZA-SC). To conduct DFT calculation for non-periodic ZSM-5 cluster, the structure was hydrogen-terminated, which suggests all terminal Si and O atoms were saturated by hydrogen atom. During the geometry optimization, the bond length of terminal O-H and Si-H were fixed at 0.95 Å and 1.50 Å, respectively. The initial structure has 96 T-sites. To satisfy the SiO_2/Al_2O_3 ratio of the catalyst, 2 tetrahedral sites were replaced by Al atom. Based on the position of silica atom, these T-sites can be classified into 12 groups, which were labelled from T1 to T12. Al atom is preferred to be located at T12 sites. Two T12 sites were occupied by Al [4]. The introduced Pt and Zn atoms are located closed to the Al to form [Al-O-Pt] since metal atoms often react with the Brönsted acid sites. Three kinds of metal locations are considered, i.e., in the large pore, in the small pore and on the external surface of the zeolite structure.

1.2 NH_3-TPD

Surface acidity measurements were performed by NH_3-TPD using ~300 mg samples in a Finesorb-3010 chemisorption analyzer. Ammonia was selected due to its simplicity, small molecular size, and ability to titrate both strong and weak acid sites on the catalyst. Prior to measurements, fresh samples were activated in 5% O_2/Ar at 600 °C for 30 min with a ramp rate of 10 °C/min. All samples were then cooled to 100 °C for adsorption of ammonia, performed using a flow of 30 sccm of 5% NH_3/N_2 for 90 min. After flowing He at 30 sccm for 1 h to remove any physically adsorbed NH_3, TPD was carried out by ramping to 600 °C at 10 °C/min increments and holding for 30 min. A thermal conductivity detector (TCD) was employed to determine the amount of desorbed NH_3.

1.3 DRIFT study on acidity

The surface acidity of the catalyst was also investigated by DRIFT spectroscopy (Nicolet iS 50) of adsorbed pyridine. The catalyst sample was put in the environmental chamber under 30 sccm N_2 flow. It was pretreated at 400 °C for 15 min before collecting background spectra at 25 °C with 512 scans at Kubelka-Munk mode. Pyridine was introduced to the sample by introducing the N_2 flow to a bubbler filled with pyridine before sending it to the environmental chamber. After introducing pyridine for 30 min, pure N_2 gas was sent to the environment chamber for another 10 min to remove the gas-phase pyridine before the spectrum was collected with 512 scans at Kubelka-Munk mode.

The acidity of the catalyst was also investigated by DRIFT spectroscopy using KBr as the background. KBr was put in the environmental chamber under 30 sccm N_2 flow. It was pretreated at 400 °C for 15 min before collecting background spectra at 25 °C with 512 scans at Kubelka-Munk mode. The catalyst sample was then put in the environmental chamber under 30 sccm N_2 flow. It was pretreated at 400 °C for 15 min before collecting sample spectra at 25 °C with 512 scans at Kubelka-Munk mode.

1.4 XRD

The crystalline phase compositions of prepared catalysts were examined by X-ray diffraction on a Rigaku Multiflex diffractometer with Cu Kα irradiation at a voltage of 20 kV and current of 40 mA in the 2θ of 3-60^o. Besides the pristine catalysts, the spent catalysts after the octane aromatization reactions were also analyzed by XRD.

2. DFT study on octane conformation

In the gaseous phase, the linear conformation of octane (Figure S5b) is 0.27 eV lower than the circular counterpart (Figure S5c), suggesting the linear is more stable. When the molecules are

absorbed in the inner pores of the catalyst, the energy gap between these conformations are narrower to 0.1~0.2 eV (Table S7), which indicates that the pore structure promotes the conformation evolution from line type to circular type, which will favor the cyclization of C_8H_X species. This phenomenon may play a role on the improved selectivity of aromatization products when the Pt atoms deposit in the inner pores in Pt-Zn/UZSM-5-I. The confined environment of the Pt atoms in the inner pore may facilitate the formation of aromatic products.

3. Acidity properties of the catalysts

3.1 DRIFT study of the catalysts

DRIFT is employed to probe not only the environment of Pt on the catalyst surface, but also the acid sites with pyridine as the probe molecule. Figure S8 shows the DRIFT spectra collected over UZSM-5, Zn/UZSM-5-II, Pt-Zn/UZSM-5-I and Pt-Zn/UZSM-5-II upon pyridine adsorption at room temperature. The peaks around 1440 cm^{-1} are assigned to Lewis acid sites [5, 6], indicating the presence of Lewis acid sites in the catalysts. The signals due to Brönsted acid sites upon pyridine adsorption at 1540 cm^{-1} [7] are weak, suggesting the weak Brönsted acidity of the catalysts. The peak located at 1483 cm^{-1} on HZSM-5 spectrum is assigned to the pyridinium H-bonded with the ZSM-5 framework, while the signal at 1588 cm^{-1} is assigned to the physisorbed pyridine [8, 9]. The peak intensities in these spectra from different samples vary from each other. The intensities on the spectrum of UZSM-5 are weak, suggesting the low concentration of acid sits. When Pt and Zn are loaded to the zeolite by WI method to form Pt-Zn/UZSM-5-I, the peaks grow stronger, indicating the increased number of acid sites upon metal loading. When Zn is introduced to UZSM-5 structure by SEA method to form Zn/UZSM-5-II, the peak intensity, particularly the peak due to Lewis acid sites, is significantly increased. The loading of Pt to form

Pt-Zn/UZSM-5-II, however, does not further enhance the peak intensity. These phenomena illustrate the stronger Lewis acidity of Zn/UZSM-5-II and Pt-Zn/UZSM-5-II compared with Pt-Zn/UZSM-I is closely related to their different Zn loading methods. The stronger Lewis acidity of Zn/UZSM-5-II may facilitate the aromatization of octane conversion, as is observed in their reaction performances.

The DRIFT spectra of the pristine Pt-Zn/Si-UZSM-5 and Pt-Zn/UZSM-5-I were also collected (Figure S9) using KBr as the background to study the OH groups. The peaks at 3745 and 3737 cm^{-1} are observed on the spectra of Pt-Zn/Si-UZSM-5 and Pt-Zn/UZSM-5-I, respectively. These peaks are assigned to the Si-OH group of the catalyst[10]. The peak due to Si-OH-Al group in Pt-Zn/UZSM-5-I, which is expected around 3600-3650 cm^{-1}, is not strong comparing with the noise signal of the curve. This phenomenon indicates the weak Brönsted acidity of the catalyst, which is in line with the observation from DRIFT study upon pyridine adsorption.

3.2 NH_3-TPD analysis of the catalysts

The features of acidic sites of these catalysts are further quantified using NH_3 temperature-programmed desorption (TPD) analysis. The results are displayed in Table S8 and Figure S10 to compare the change using different support materials and metal modification methods. The desorption pattern of NH_3 at elevated temperatures indicates the strength of various acidic sites where NH_3 molecules are absorbed. The peak deconvolution indicates acidic sites with various strengths resulting in NH_3 desorption at low, medium and high temperatures with peaks at approximately 250, 350 and 500 ^oC, respectively. The peaks at higher temperatures are associated with NH_3 molecules desorbed from stronger surface acid sites. After quantification, the total acid amounts for UZSM-5, Pt/UZSM-5, Pt-Zn/UZSM-5-I, Pt-Zn/UZSM-5-II and Pt-Zn/HZSM-5 catalysts are determined to be 94, 156, 521, 601 and 1149 μmol NH_3/g_{cat}, respectively. The strong

acidity of Pt-Zn/HZSM-5 may explain the high octane conversion along with the production of C_9-C_{12} aromatics from octane conversion. The acidity of UZSM-5, on the other hand, is much weaker. The introduction of Pt to UZSM-5 structure results in a NH_3 desorption peak at low temperature. The acidity is significantly enhanced when Zn is loaded to the catalysts, which may improve their catalytic activity in the octane aromatization reaction.

When comparing the NH_3-TPD curves, a peak at 300 ^oC is clearly presented on the curve of Pt-Zn/UZSM-5-I, which is not witnessed on the curve of Pt-Zn/UZSM-5-II. This change features the different chemical environment of the acid sites in Pt-Zn/UZSM-5-I and Pt-Zn/UZSM-5-II, which is in line with the different acidity of the catalysts demonstrated by DRIFT study upon pyridine adsorption. The difference of their total acid numbers is not really so prominent considering their dramatically different catalytic activities in octane aromatization. The improved catalytic performance of Pt-Zn/UZSM-5-II is probably mainly due to the altered chemical environment of the metal sites, rather than the increased acid concentration in the catalyst.

4. XRD study of the catalysts

The crystallinity of the catalysts is examined through powder X-ray diffraction (Figure S11). The planes revealed by XRD patterns are compared to the zeolite fringe images obtained by the TEM analysis. Some of them are shown in Figure S7. The widths of the fringes of the obtained TEM are measured as 9.65, 10.05, 10.83, 10.9, 10.95, 11.1 and 11.2 Å, By comparing the fringe width with the d-space of ZSM-5, these lattice structures are assigned to the (011), (020), (200) and (111) planes, which are also corresponding to the major peaks on the XRD spectra. The results may illustrate that these planes constitute a large portion of the ZSM-5 zeolite lattice. It is observed that the ZSM-5 crystalline structure remains intact upon metal modification and the reactions. However, it is also noted that the diffraction peaks due to the (011), (200), (020), (301) and (040) crystal

planes of the Pt and Zn modified catalysts are weaker than those of the HZSM-5. On the contrary, increased peak intensity due to (011), (200) and (020) planes is witnessed when Pt and Zn are loaded to UZSM-5. The peak intensity changes may be attributed to the changed crystallinity of these planes upon introducing the metal species to the catalysts. Pt and Zn species probably end up with different sites on HZSM-5 and UZSM-5, resulting in distinguished XRD peak intensity variations.

5. Tables

Table S1. Product selectivity of octane conversion over various catalysts

Catalyst	**UZSM-5**	**Zn/UZSM-5-I**	**Zn/UZSM-5-II**	**Pt-Zn/UZSM-5-II (N_2)**
Octane conversion	3.7	5.5	5.8	98.1
Benzene	0	0	0.1	5.3
Toluene	0.7	0.4	0.5	8.8
Xylenes	0.5	0.6	0.9	51.4
C_9–C_{12} aromatics	0.3	0.2	0.5	2.0
Naphthalene derivatives	0	0	0	0.3
C_6-C_7 alkanes	3.3	2.6	2.0	3.8
C_8 alkanes	77.1	71.4	79.6	1.7

* Reactions are carried at 400 ^oC under 2.5 MPa CH_4 for 1 h

Table S2. Conversions of feedstocks and yields of aromatics during octane aromatization over Pt and Zn modified catalysts

Condition	CH_4 conversion/%	Ethane selectivity/%	Butane selectivity/%	Liquid yield/%	Gas product selectivity/%
Pt-Zn/UZSM-5-I	0.2	6.2	6.7	89	18.3
Pt-Zn/UZSM-5-II	0.5	3.7	9.2	81	19.9
Pt-Zn/UZSM-5-II (N_2)	-	2.5	16.2	74	26.7
Pt-Zn/HZSM-5	1.1	31.7	7.6	48	51.9
Pt-Zn/UZSM-5-I/SiO_2	0.2	5.0	6.7	92	14.1
Pt-Zn/UZSM-5-II/SiO_2	0.4	2.5	10.8	82	21.2
Pt-Zn/HZSM-5/SiO_2	1.0	29.8	6.0	50	50.6
Pt-Zn/UZSM-5-III	0.2	4.2	12.0	81	24.6
Pt-1%Zn/UZSM-5-II	0.3	2.5	10.7	83	18.8
Pt-3%Zn/UZSM-5-II	0.3	3.4	10.9	81	19.8
Pt-Zn/UZSM-5-II (inner pore blocked)	0.1	5.6	7.8	87	20.5

*The error values of methane conversions, selectivity and liquid yields are 0.3%, 0.3% and 1% respectively

**Liquid yield is the ratio between the mass of collected liquid after reaction and the mass of octane feedstock

Table S3. Selectivity of C_9-C_{12} aromatics with single phenyl ring and naphthalene derivatives from octane aromatization over various catalysts

Catalyst	C_9–C_{12} aromatics				Naphthalene derivatives		
	C_9	C_{10}	C_{11}	C_{12}	C_{10}	C_{11}	C_{12}
Pt/UZSM-5	0.5	0	0	0	0	0	0
Pt-Zn/UZSM-5-I	0.6	0	0	0	0.2	0	0
Pt-Zn/UZSM-5-II	2.1	0.2	0	0	0.3	0.1	0
0.5%Pt-Zn/UZSM-5-II	0.8	0.1	0	0	0.3	0	0
Pt-Zn/HZSM-5	5.4	3.1	2.1	0.8	2.5	1.3	0.7
Pt-Zn/UZSM-5-I/SiO_2	0.4	0.1	0	0	0.2	0	0
Pt-Zn/UZSM-5/SiO_2-I	0.3	0	0	0	0.2	0	0
Pt-Zn/UZSM-5-II/SiO_2	0.5	0.2	0	0	0.4	0.1	0
Pt-Zn/UZSM-5/SiO_2-II	1.4	0.9	0.4	0	0.3	0	0
Pt-Zn/HZSM-5/SiO_2	6.1	1.2	0.5	0.4	2.0	0.9	0.5
Pt-1%Zn/UZSM-5-II	0.2	0	0	0	0	0	0
Pt-3%Zn/UZSM-5-II	0.9	0.5	0	0	0	0	0
Pt-Zn/UZSM-5 (pore blocked)	11.3	3.2	0.8	0	0	0	0
Pt-Zn/UZSM-5-III	0.2	0	0	0	0	0	0

* Reactions are carried at 400 ^oC under 2.5 MPa CH_4 for 1 h

Table S4. Detailed EXAFS fitting parameters of Pt/UZSM-5, Pt-Zn/UZSM-5-I, and Pt-Zn/UZSM-5-II

	Pt-UZSM-5	Pt-Zn/UZSM-5-I	Pt-Zn/UZSM-5-II
ΔE_0 (eV)	8.5 ± 2.6	8.8 ± 2.3	9.6 ± 0.7
CN_O	2.9 ± 0.6	4.4 ± 1.3	4.0 ± 0.9
CN_{Pt}	2.8± 1.3	1.3 ± 0.8	1.5 ± 1.0
r_O (Å)	2.04 ± 0.02	2.03 ± 0.02	2.04 ± 0.1
r_{Pt} (Å)	2.67 ± 0.02	2.60 ± 0.044	2.62 ±0.05
σ^2 ($\times 10^{-3}$ Å^2)	1 ± 4	5 ± 4	3 ± 4

Table S5. Metal dispersion of Pt in different catalysts

Catalyst	Metal dispersion
Pt-Zn/HZSM-5	75
Pt/UZSM-5	44
Pt-Zn/UZSM-5-I	51
Pt-Zn/UZSM-5-II	87
Pt-Zn/UZSM-5-II (0.5%Pt)	92

Table S6. Theoretical calculation results on the Pt-Zn/HZSM-5 with Pt atom in inner pore or the Pt atom on external surface

Metal	Energy/hartree			ΔE comparing with external surface/ (kJ/mol)	
	External surface	10-ring	5-ring	10-ring	5-ring
Pt	-59320.244	-59320.263	-59320.275	-49	-81
Zn	-43770.082	-43770.292	-43770.284	-546	-525

Table S7. Theoretical calculations results (eV) of octane dehydrogenation over the Pt(111) plane on external surface and the Pt_8 cluster in inner pore of the catalyst (400 ^oC/30 kPa)

Reaction	Equation	Pt(111)			Pt_8		
		Ea	**ΔE**	**ΔG**	**Ea**	**ΔE**	**ΔG**
R1	$C_8H_{18} = C_8H_{18}$*		-1.45	-0.03		-0.87	0.55
R2A	C_8H_{18}* = 1-C_8H_{17}* + H*	0.91	0.20	0.20	0.79	0.33	0.33
R2B	C_8H_{18}* = 2-C_8H_{17}* + H*	0.68	0.06	0.06	0.77	0.40	0.40
R3A	1-C_8H_{17}* = 1-C_8H_{16}* + H*	0.76	-0.05	-0.05	0.79	0.39	0.39
R3B	2-C_8H_{17}* = 1-C_8H_{16}* + H*	0.89	0.09	0.09		0.32	0.32
R4	1-C_8H_{16}* = 1-C_8H_{16}(g)		2.16	0.74		1.41	-0.22
R5	2H*= H_2(g)		0.87	-0.20		0.70	-0.37

*Favorable pathway is R1-R2B-R3B-R4-R5

Table S8. Theoretical calculations results (eV) of octane in linear and circular conformations in different positions of ZSM-5 framework

Absorption position	**Linear conformation energy / eV**	**Circular conformation energy / eV**
10-member ring	-2440.79	-2440.66
12-member ring, Z-shape tunnel	-2440.89	-2440.69
Tunnel cross of 10-member ring	-2440.91	-2440.75
Tunnel cross of 12-member ring	-2441.03	-2440.75

Table S9. The acidity of the catalysts (μmol NH_3/g catalyst)

Samples	Weak acid sites	Medium acid sites	Strong acid sites	Total
UZSM-5	73	17	4	94
Pt/UZSM-5	156	0	0	156
Pt-Zn/UZSM-5-I	393	128	0	521
Pt-Zn/UZSM-5-II	324	277	0	601
Zn-Pt/HZSM-5	633	616	0	1149

6. Figures

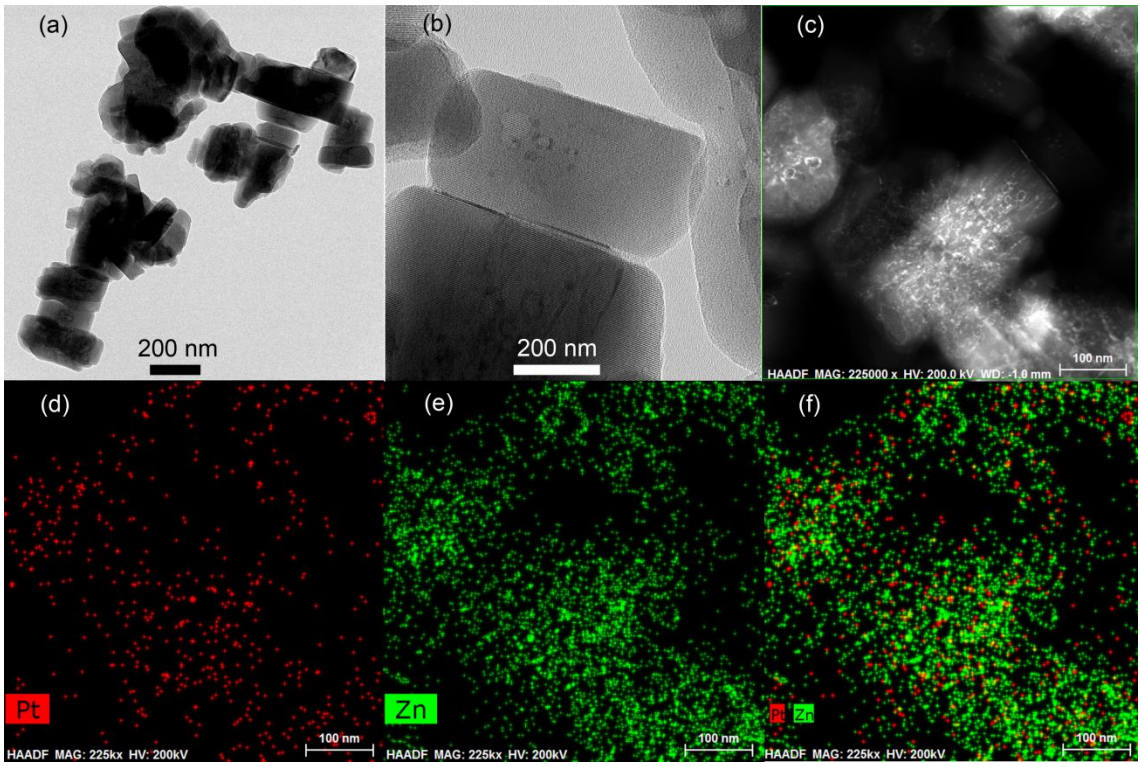

Figure S1. TEM images of Pt-Zn/HZSM-5 particles (a-b). The high-angle annular dark-field (HAADF) scanning TEM images of the particles are shown in c. The element mapping results of the particles in (c) are displayed in d-f, where Pt and Zn are in red and green, respectively

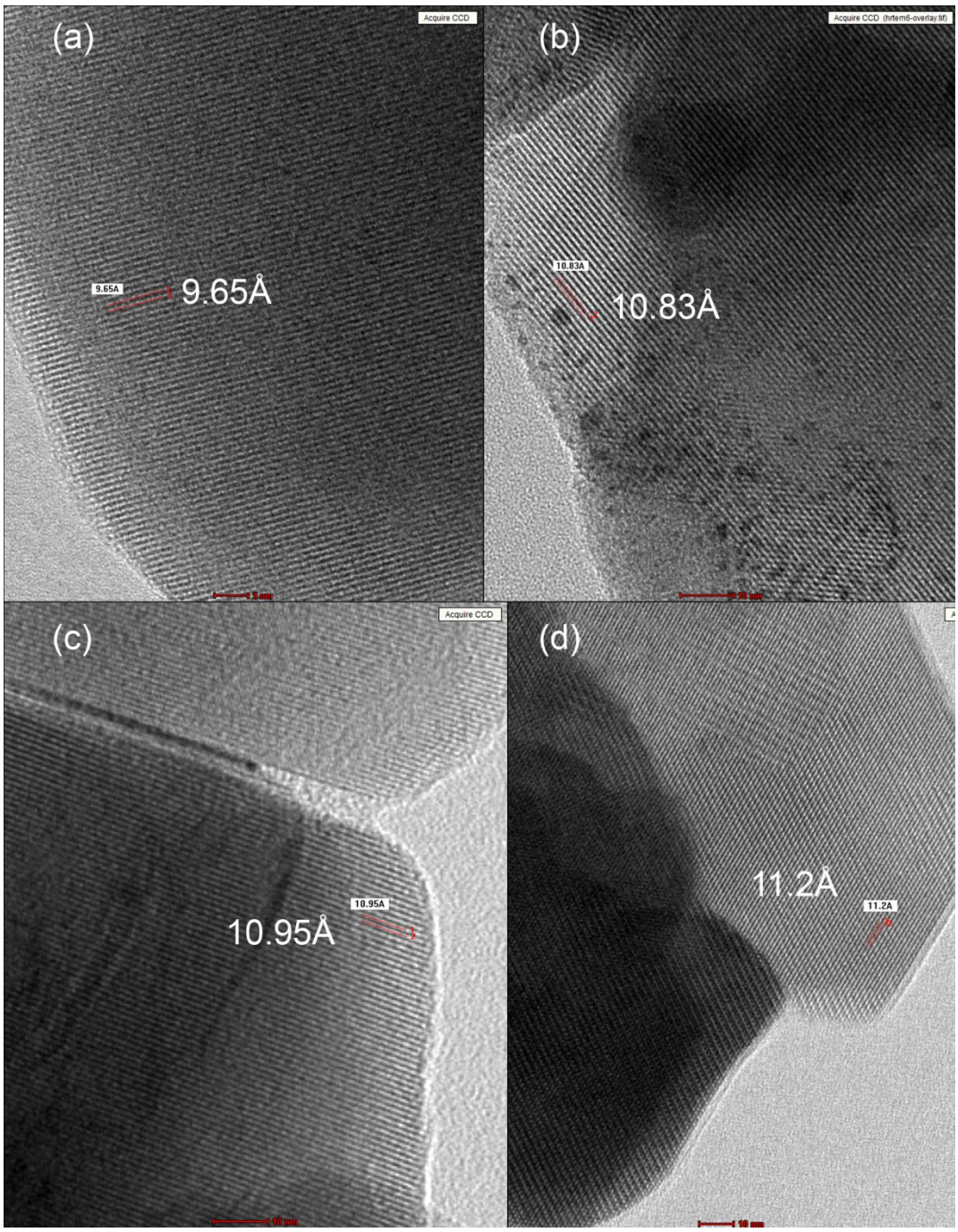

Figure S2. Fringe structures in TEM images of Pt-Zn/U-ZSM-5-I (a), Pt-Zn/U-ZSM-5-II (b) and Pt-Zn/HZSM-5 (c-d) catalysts

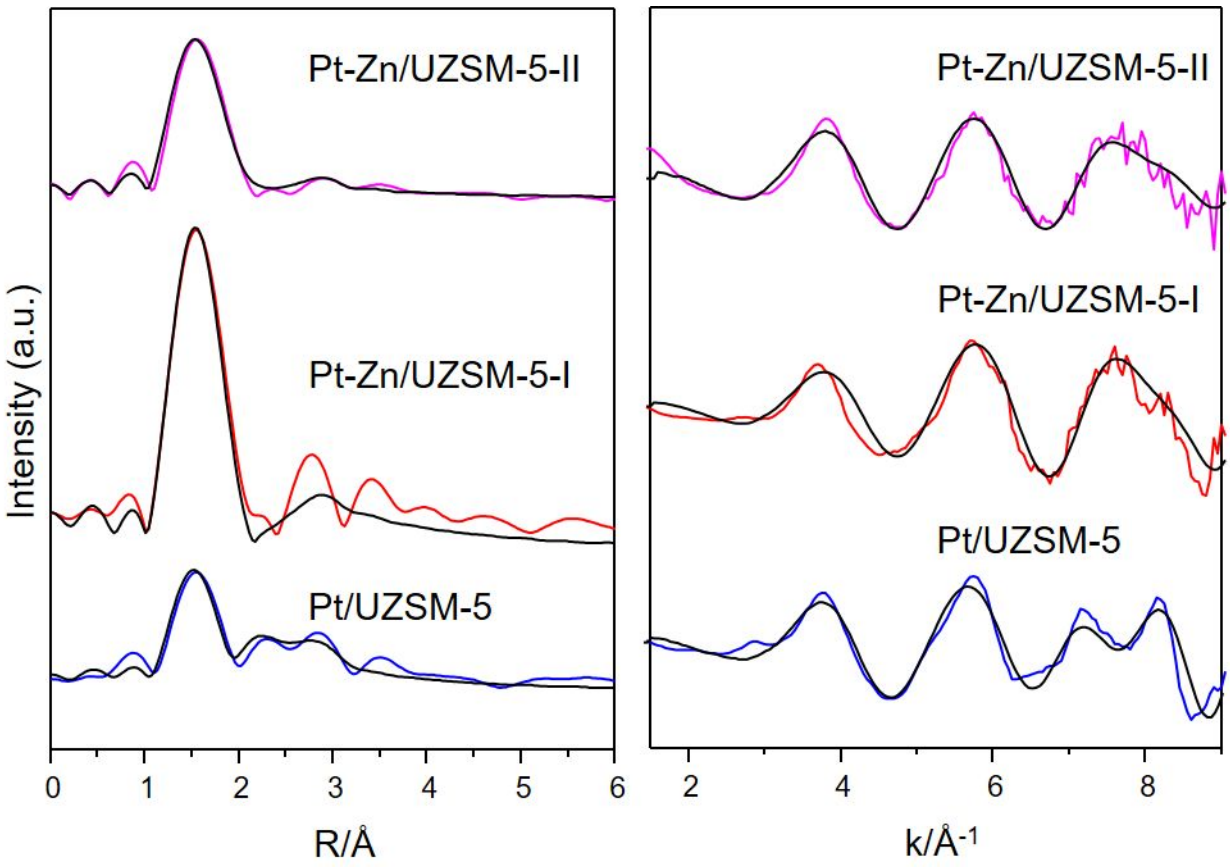

Figure S3. The fitted EXAFS spectra in R-space (a) and k-space (b) of Pt/UZSM-5, Pt-Zn/UZSM-5-I and Pt-Zn/UZSM-5-II. Fitted spectra are shown in black curves

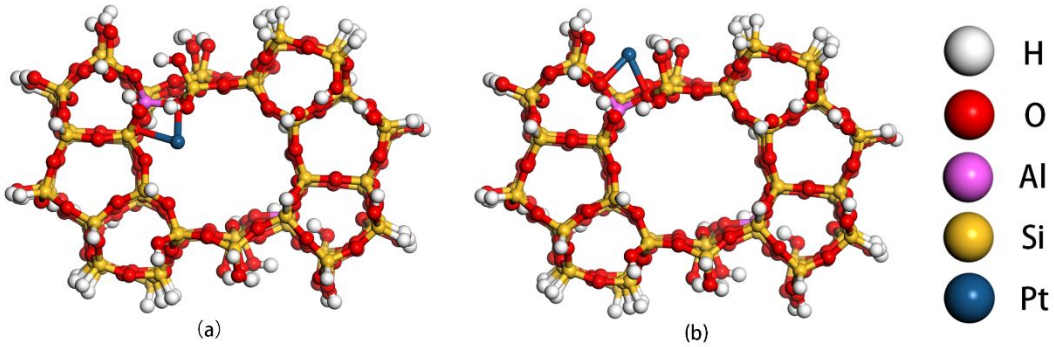

Figure S4. ZSM-5 structure with Pt in inner pore (a) and on the external surface (b)

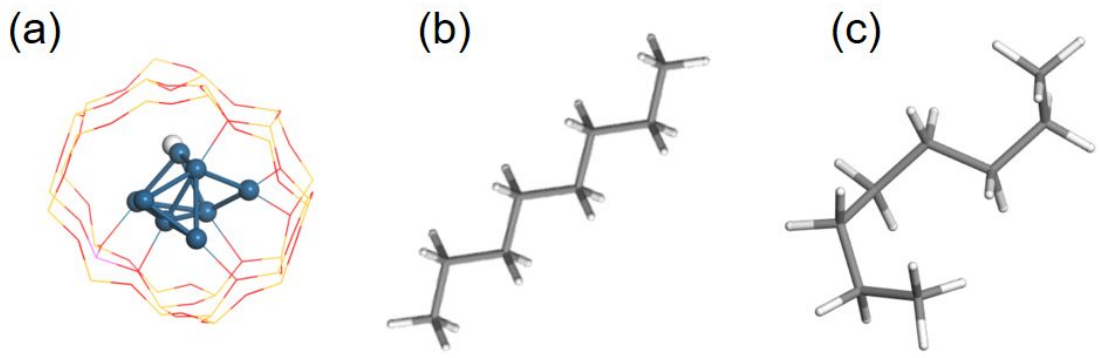

Figure S5. Pt_8 clusters in ZSM-5 inner pore (a) with Si and O shown in yellow and red, respectively. The linear (b) and circular (c) conformation octane molecule

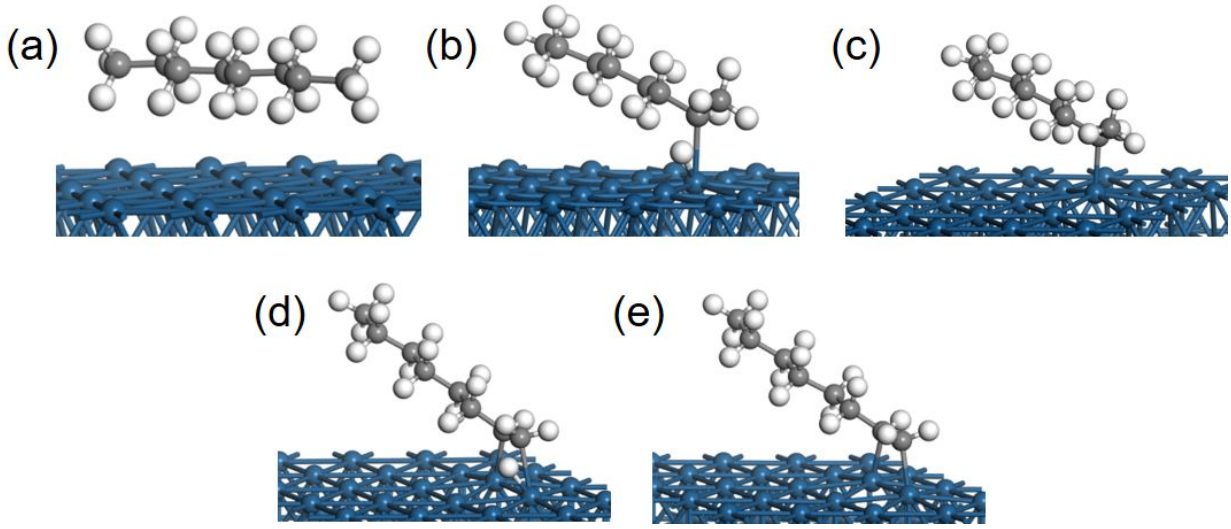

Figure S6. Reaction and transition state intermediates such as C_8H_{18}* (a), TS1 (b), 2-C_8H_{17}* (c), TS2 (d) and 1-C_8H_{16}* (e) absorbed on Pt(111) plane

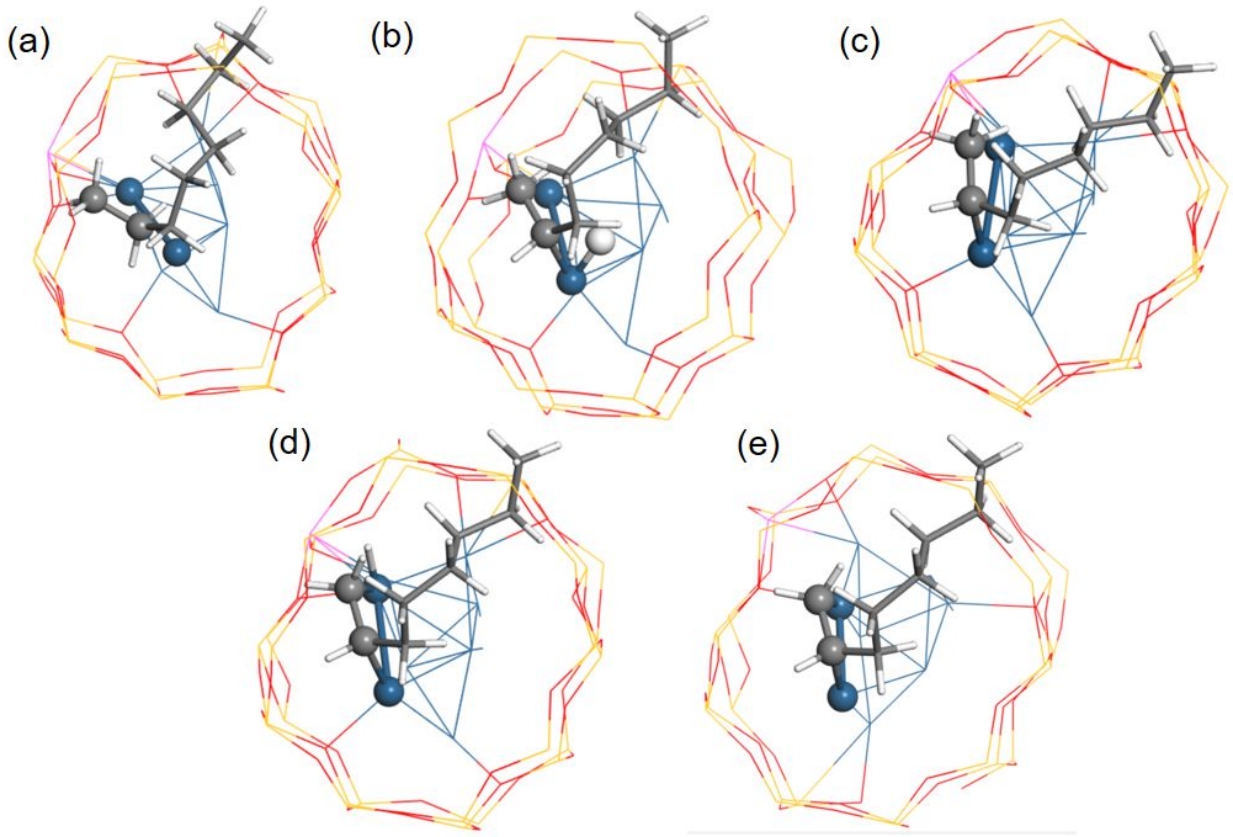

Figure S7. Reaction and transition state intermediates such as C_8H_{18}* (a), TS1 (b), 2-C_8H_{17}* (c), TS2 (d) and 1-C_8H_{16}* (e) absorbed on Pt_8 cluster in ZSM-5. Si and O atoms are shown in yellow and red, respectively.

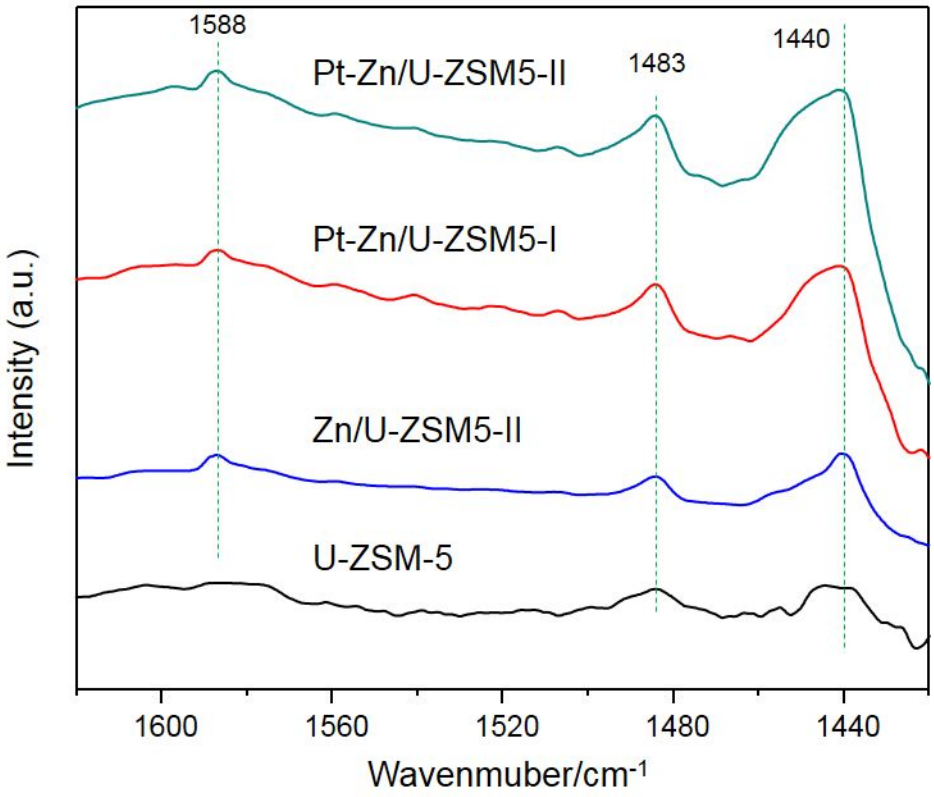

Figure S8. DRIFT spectra of the catalysts upon pyridine adsorption

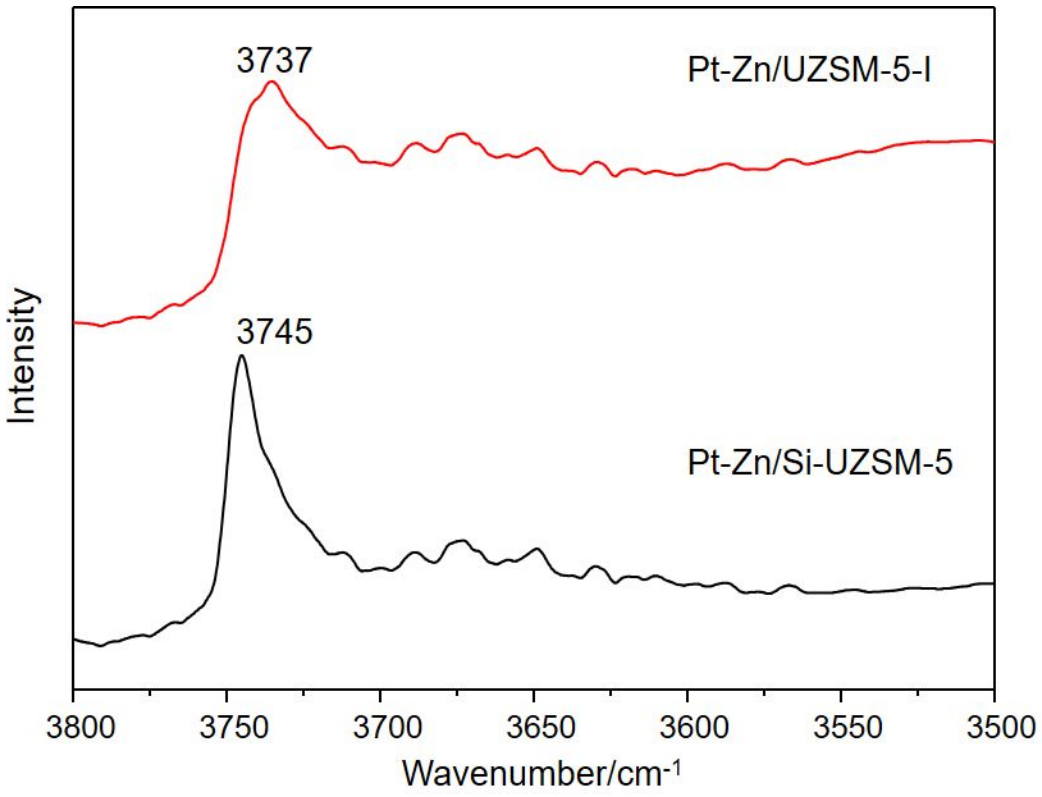

Figure S9. DRIFT spectra of Pt-Zn/Si-UZSM-5 and Pt-Zn/UZSM-5-I

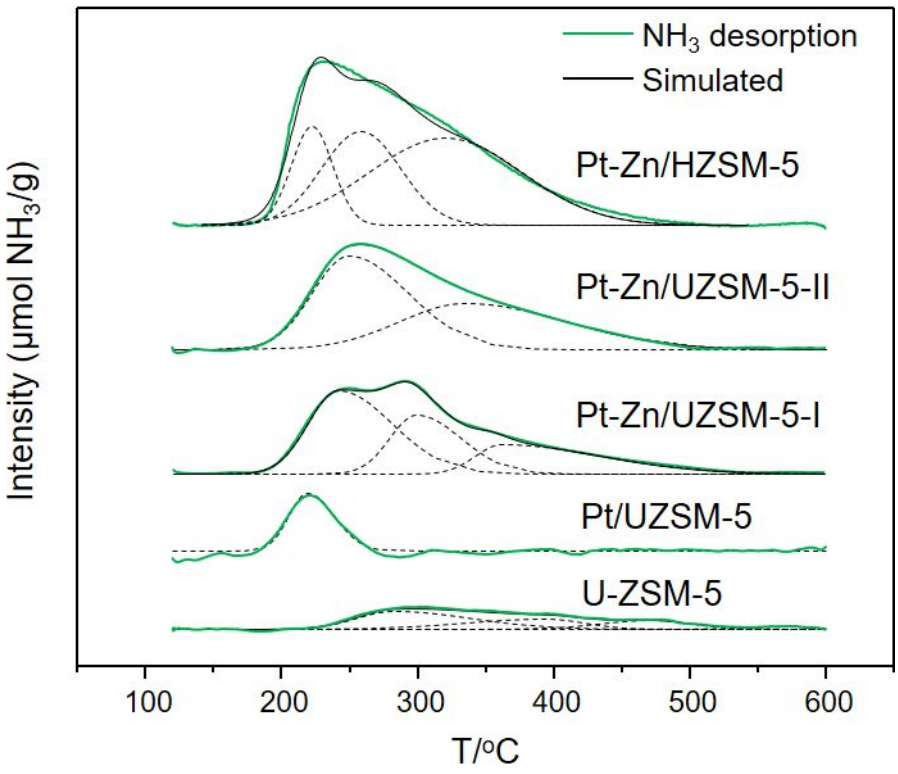

Figure S10. NH_3-TPD analysis results of catalysts

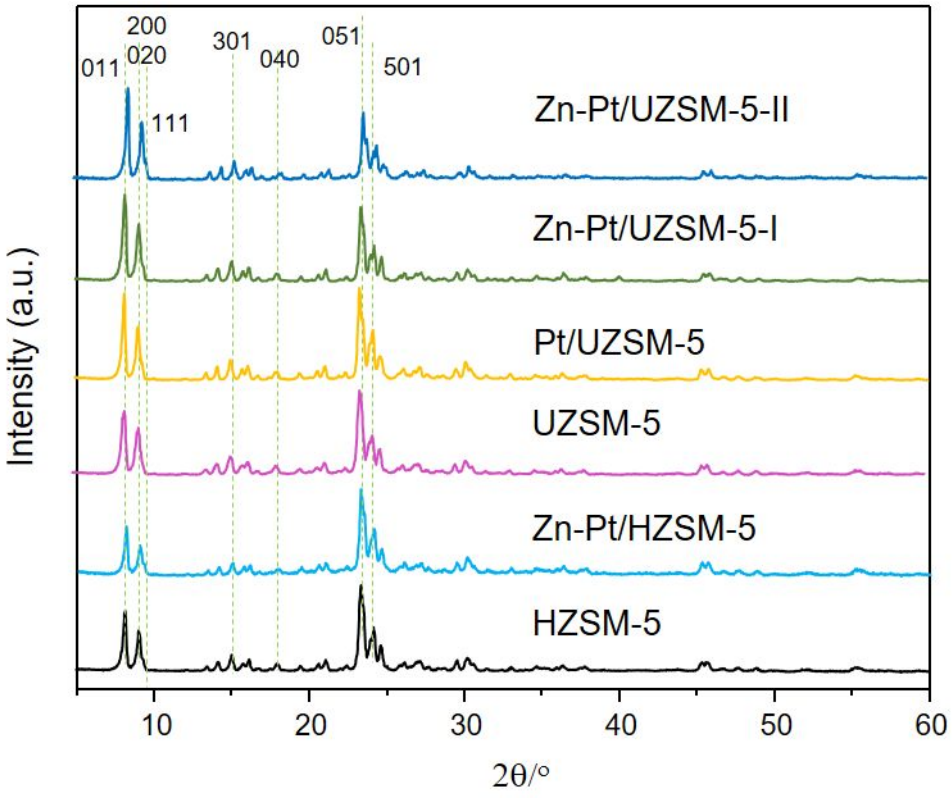

Figure S11. XRD spectra of the pristine catalysts

7 References

[1] Stepanov, A.G., Arzumanov, S.S., Gabrienko, A.A., Parmon, V.N., Ivanova, I.I., Freude, D., Significant influence of Zn on activation of the C-H bonds of small alkanes by Bronsted acid sites of zeolite, Chemphyschem : a European journal of chemical physics and physical chemistry, **2008**, *9*, 2559-2563.

[2] Weaver, J.F., Surface chemistry of late transition metal oxides, Chem. Rev., **2013**, *113*, 4164-4215.

[3] Gao, J., Zheng, Y., Tang, Y., Jehng, J.-M., Grybos, R., Handzlik, J., Wachs, I.E., Podkolzin, S.G., Spectroscopic and Computational Study of Cr Oxide Structures and Their Anchoring Sites on ZSM-5 Zeolites, ACS Catal., **2015**, *5*, 3078-3092.

[4] Fripiat, J.G., Berger-Andre, F., Andre, J.-M., Derouane, E.G., Non-empirical quantum mechanical calculations on pentasil-type zeolites, Zeolites, **1983**, *3*, 306-310.

[5] Almutairi, S.M.T., Mezari, B., Pidko, E.A., Magusin, P.C.M.M., Hensen, E.J.M., Influence of steaming on the acidity and the methanol conversion reaction of HZSM-5 zeolite, J. Catal., **2013**, *307*, 194-203.

[6] Yi, D., Huang, H., Meng, X., Shi, L., Adsorption–desorption behavior and mechanism of dimethyl disulfide in liquid hydrocarbon streams on modified Y zeolites, Appl. Catal. B Env., **2014**, *148-149*, 377-386.

[7] Xu, W., Miller, S.J., Agrawal, P.K., Jones, C.W., Zeolite topology effects in the alkylation of phenol with propylene, Appl. Catal. A Gen., **2013**, *459*, 114-120.

[8] Buzzoni, R., Bordiga, S., Ricchiardi, G., Lamberti, C., Zecchina, A., Interaction of Pyridine with Acidic (H-ZSM5, H-β, H-MORD Zeolites) and Superacidic (H-Nafion Membrane) Systems: An IR Investigation, Langmuir, **1996**, *12*, 930-940.

[9] Glazunov, V.P., Odinokov, S.E., Infrared spectra of pyridinium salts in solution-I. the region of middle frequencies, Spectrochim. Acta, **1982**, *38A*, 399-408.

[10] Derouane, E.G., Védrine, J.C., Pinto, R.R., Borges, P.M., Costa, L., Lemos, M.A.N.D.A., Lemos, F., Ribeiro, F.R., The Acidity of Zeolites: Concepts, Measurements and Relation to Catalysis: A Review on Experimental and Theoretical Methods for the Study of Zeolite Acidity, Catal. Rev., **2013**, *55*, 454-515.